Research in Astronomy and Astrophysics, 22:045013 (16pp), 2022 April
https://doi.org/10.1088/1674-4527/ac56cc

The Response of the Earth’s Lower Ionosphere to Gamma-Ray Solar Flares and their Associated X-ray

Mahmoud Mohery[1], Hussein M. Farid[2], and Alaa Ali[2,3]
[1] Dept. of Phys, College of Science, University of Jeddah, Jeddah, Saudi Arabia; mmohery@uj.edu.sa
[2] Astronomy, Space Science & Meteorology Department, Faculty of Science, Cairo University, Giza 12613, Egypt; hfarid@sci.cu.edu.eg
[3] Astronomy Dept., Faculty of Science, King Abdulaziz University, 21589 Jeddah, Saudi Arabia; afouad@sci.cu.edu.eg
Received 2022 January 5; revised 2022 February 14; accepted 2022 February 16; published 2022 March 17

Abstract

The present work aims to explore the impact of solar gamma-ray flares (GRFs), detected by the Fermi-Large Area Telescope (LAT), and their associated X-ray flares (XRFs) on the Earth’s lower ionosphere. The data of ionospheric parameter fmin were collected from the Yamagawa mid-latitude ionosonde station in Japan. Because most of the GRFs used in this study are associated with soft X-ray (SXR) emissions, detected by the Geostationary Operational Environmental Satellite (GOES), we classified them into three types: simultaneous (S), delayed (D) and not associated (N), reflecting the phase occurrence of the solar flares. Generally, the ionospheric D layer responds strongly to XRFs more than GRFs. The temporal profiles of the ionospheric parameter fmin show distinct behaviors as a response to the various GRF types. In the case of the S-type, a single strong peak, with an average value of 5.2 MHz, emanates in the fmin profile within an average interval of time of less than half an hour. In the case of the D-type, two successive peaks appear in the fmin profile, with an average value of 6.0 MHz for the second peak through a time interval of one hour after the onset of gamma-ray (GR) emissions. The response of the fmin parameter to the N-type flares appears as a single peak with an average value of 4.8 MHz within about an hour. We notice that the difference between the fmin peak values and the corresponding reference ones (dfmin) is more convenient and representative than the fmin values, where the median GR flux of the S-, D- and N-types tends to increase as the average dfmin increases.

Key words: Sun: X-rays – gamma-rays – Earth: ionosphere – satellites

1. Introduction

The Sun is the major source of several hazards in Earth’s space environment. Solar storms, e.g., coronal mass ejections (CMEs) and solar flares (SFs), have a substantial impact on space weather, like the ionospheric storms that occur in Earth’s upper atmosphere (Farid et al. 2015, 2020; Guyer & Can 2013). In fact, ionospheric storms can cause troubles that lead to disturbances in space-based technologies, e.g., radio blackout and Global Positioning System (GPS) signal inaccuracies (Moldwin 2008). SFs are violent phenomena that produce electromagnetic energy in the range of radio waves to gamma-rays (GRs). The source of this energy is assumed to be magnetic energy held in the solar corona, which is released during the magnetic reconnection (Kafexhiu et al. 2018). The first and successive detections of GRs with energies >10 MeV, which were observed by the Solar Maximum Mission (SMM) spectrometer, revealed evidence of pion-decay emission and the multiple phases of SFs (Chupp et al. 1982; Forrest et al. 1985, 1986). The Energetic Gamma Ray Experiment Telescope (EGRET) on board the Compton Gamma Ray Observatory captured the first GeV gamma-ray flares (GRFs, Vilmer et al. 2003). Most of the SFs detected by EGRET, with energies ranging from 50 MeV to 2 GeV, last tens of minutes. However, there were two eruptions that lasted several hours, giving rise to a new class of flares known as long-duration GRFs (Ryan 2000; Chupp & Ryan 2009). SOL2012-03-07, a GOES X-class flare that lasted almost 20 hr, is the longest emission ever detected (Ajello et al. 2014). Kouloumvakos et al. (2020) examined the solar eruptive event on 2017 September 10 that produced long-lasting GR emission. They suggested that the origin of the high-energy ions that produce late-phase GR emission remains obscure, however the acceleration of protons at coronal shocks, caused by CMEs, may be an explanation.

Ajello et al. (2021) presented the first catalog of SFs that were detected by the Fermi-Large Area Telescope (LAT). This database contains about 90 individual SFs that occurred over 42 days spanning between 2010 and 2018, with GR energies ranging from 30 MeV to 10 GeV. They noticed that 37 flares exhibited delayed emission beyond the prompt-impulsive hard X-ray (HXR) phase. Of these, 21 indicate delayed emissions for more than two hours. The Fermi observations of SFs revealed a wealth of various flares, ranging from short prompt-impulsive (Ackermann et al. 2012) to gradual-delayed long-duration flares (Ackermann et al. 2014). Ajello et al. (2014)

reported the detection of two bright X-class SFs on 2012 March 7 with GR energies of up to 4 GeV, indicating both are impulsive and temporally extended emission phases. They found the GRs and X-rays (XRs) associated with these flares appear to come from the same active location. In addition, the flux of GRs (with energies >100 MeV) during the first hour (impulsive phase) decreased monotonically, followed by a gradual reduction over the next 20 hr.

Qian et al. (2019) used model simulations and data analysis to evaluate the effect of SFs on the coupled thermosphere and ionosphere (TI) system. This analysis was based on observations of multiple SFs and a major geomagnetic storm that occurred during the interval of 2017 September 6–11. The two largest flares, X9.3 and X8.2, were disk and limb flares, respectively. They suggested that the response of the lower thermosphere and E region of the ionosphere is unaffected by the flare location, while above 150 km the TI system responds more strongly to disk flares than to limb flares. In addition to the previous study, Yamauchi et al. (2018) discussed the ionospheric response for two XRFs (X2.2 and X9.3) that occurred on 2017 September 6 and 8. The two flares were accompanied by two interplanetary CMEs that arrived on Earth, as well as increases in the energetic particle flux in both the solar wind and the inner magnetosphere. Both flares increased the ionospheric electron density for roughly 10 min. Moreover, the X9.3 flare raised the temperatures of the electrons and ions, over 69°–75° geomagnetic latitude, until the XR flux dropped below the level of X-class flares.

Further, away from the solar system, some evidence suggests that GRFs from extrasolar sources can trigger ionospheric disruptions. Inan et al. (2007) demonstrated that emission of the giant GRF from the magnetar SGR 1806–20, on 2004 December 27, created significant disturbances in the daytime lower ionosphere, leading to unusual variations in the amplitude/phase of the propagating very low frequency (VLF) signals. In addition, Tanaka et al. (2008) highlighted that on 1998 August 27, severe disturbances in the lower ionosphere occurred as a result of a soft GRF emission from the SGR 1900+14 source, an unusual neutron star located near the Galactic center.

The ionospheric D layer is the innermost layer of the ionosphere, located 50–90 km above the Earth's surface, while the F layer is the uppermost region of the ionosphere at over 160 km altitude. The D layer disappears at night and plays a critical role in the propagation of radio-wave signals at low and extremely low frequencies (below 300 kHz). The F layer, which splits into F1 and F2 layers during the daytime and merges into a single layer at night, is distinguished by the highest concentration of free electrons that play a major role in reflecting high-frequency radio waves up to roughly 35 MHz. Based on a study of the impact of ten X-class flares, detected by Geostationary Operational Environmental Satellite (GOES) during the maximum phase of solar cycle 23 between 2000 and 2004, on the D and F layers of the ionosphere, Tripathi et al. (2011) found a direct correlation between the XR intensity and both the minimum frequency of the D layer (fmin) and the maximum number density of electrons in the F2 layer (NmF2). This correlation seems to be much stronger for the D layer than the F layer. Because HXR is more energetic than SXR and extreme ultraviolet (EUV, <1 nm), it penetrates deeply into the lower ionosphere, potentially causing ionization enhancement in the D layer (Hargreaves 1992). Consequently, the D region disturbances are mainly affected by HXRs. As a result, GRFs are more likely to affect the D region because they have higher energy than HXRs. Bello et al. (2017) reported that there is a relationship between fmin and the electron density of the D-region (NmD) predicted by the IRI-2012 model. Furthermore, Barta et al. (2019) declared that there is a probable correlation between the electron concentrations of the D layer and the ionospheric parameter fmin. Therefore, we have decided to use the fmin parameter, in addition to the critical frequency of the F2 layer (foF2), to explore the influence of the GRFs on the lower and upper ionosphere, respectively.

The objective of the present work is to study the impact of solar LAT-GRFs and their associated GOES-XRFs on the (sunlit) ionosphere at middle latitudes. This will be achieved by analyzing the ionospheric fmin parameter, measured at a certain ionosonde station, in a systematic manner.

Section 2 discusses the data sources and methodology, while Section 3 displays the impact of simultaneous, delayed and not associated GRFs on the ionosphere. We display the impact of individual XRFs on the ionosphere in Section 4, while the effect of the LAT-GRF characteristics on the fmin peak values is presented in Section 5. Section 6 discusses the occurrence of GRFs and XRFs, as well as the similarities and differences in their effects on the lower ionosphere, while we draw our conclusions in the last section.

2. Data Sources and Methodology

2.1. Data Sources

In this study, we use four sets of data spanning between 2011 and 2017: (1) solar GRFs detected by the Fermi-LAT; (2) solar GRFs detected by the Fermi Gamma-Ray Burst Monitor (GBM); (3) XR flares detected by GOES; and (4) ionospheric parameter fmin detected by the mid-latitude ionosonde station in Yamagawa, Japan (YG431, the geographic latitude is 31.20° N and the geographic longitude is 130.62°E). The Fermi space telescope was launched in June 2008 in order to observe and detect high energy phenomena in the universe, particularly those of solar origin, primarily SFs. There are two instruments on board the Fermi telescope, which are the LAT and GBM. The GBM device monitors the low energy spectrum, which ranges from 8 keV to 1 MeV and the higher energy range, which ranges from about 200 keV to 40 MeV. The LAT sensor is sensitive to GR photons with energies ranging from about

20 MeV to 300 GeV. The GR and XR SF data used in this study were collected from the recent catalog presented by Ajello et al. (2021). The ionospheric data are obtained from the World Data Center (WDC) for Ionosphere and Space Weather, operated by the National Institute of Information and Communications Technology (NICT).

2.2. Methodology

To investigate the influence of GR and XR SFs on the ionospheric parameter fmin, we initially convert the GR and XR SF times from Universal Time (UT) to Japan Standard Time (JST) by adding the time zone value (+9). To compare the times of the GR and XR flares to those of the relevant ionospheric parameters, looking for the flaring events that occurred entirely in the dayside ionosphere, we followed the method described by Meeus (1998, Chapter 15). Among the Fermi-LAT SF data listed in the catalog of Ajello et al. (2021), we analyze here 30 events that affected the dayside ionosphere and have available ionospheric parameter data. Tsurutani et al. (2009) reported that the impact of solar photons on the ionosphere takes about one hour, whereas that of solar energetic particles takes from one hour to several days. We found that the ionospheric response to most Fermi-LAT flares takes roughly an hour, which agrees with Tsurutani et al. (2009)'s finding, but a few events take slightly longer than an hour.

To verify the effect of GRFs on the ionosphere on the day of the event, we compare the daily fmin profile of the event day to a reference fmin profile, which is the average of the corresponding day of the event and a day before and after it, in the preceding year and subsequent year of the event. For better analysis, we calculate the difference between the fmin and reference peak values (dfmin). The criterion we have used to identify the GRF-induced peak of the ionospheric parameter was to select the first enhancement of the ionospheric parameter within 90 minutes of the event start time, where the lowest value of the fmin peak is at least an order of magnitude above the background reference profile.

In fact, the ionospheric daily profile is characterized by the presence of many fluctuations expressing variations in electron density. The great enhancements in the electron density, or spikes, are primarily attributable to additional ionization processes that occur as a result of transient phenomena with or without a solar origin. Seeking to explain the fmin peaks that appear in the event daily profiles and are not attributed to the LAT detector, we find most of them are attributed to other events detected by the GOES and GBM detectors.

In this work, we conduct an analysis of the influence of the GRFs that were detected by the Fermi-LAT Sun monitor and their associated GOES XRFs on Earth's ionosphere. Table 1 lists 30 GRFs that occurred across 23 days between 2011 and 2017, along with some of their characteristics, e.g., start time, exposure and flux. Further, the table displays the dfmin as well as the fmin peak values and their times and intervals (the time span between the event start time and the time of fmin peak.)

In the Appendix, we present the daily profiles of the fmin parameter during the 23 event days that were discussed in this study. Each graph shows the time (JST) on the *X*-axis and the fmin daily variation (in black) on the *Y*-axis. The three dashed vertical black lines indicate the sunrise, noon and sunset times at the ionosonde station. On each fmin daily profile, the reference (background) profile (in blue) is displayed to exhibit the effect of daily variation and to maintain the seasonal variation as well. Further, the residual between the fmin and reference daily profiles is indicated (in green). The fmin peaks that are attributed to the effect of the LAT, GBM and GOES flares are shown by blue, red and black arrows, respectively. The start times of the LAT, GBM and GOES events are indicated by solid blue, red and black vertical lines, respectively. According to the findings of Barta et al. (2019), the magnitude of the fmin peak value that is attributed to the XR SF is dependent on the solar zenith angle of the detecting ionosonde station. As a result, the amplitudes of the fmin peaks that appear in the fmin daily profiles depend on the magnitude of the solar zenith angle of the Yamagawa ionosonde station.

3. The Impact of S, D and N Type GRFs on Earth's Ionosphere

The GR emission from SFs appears to affect the ionosphere in a manner comparable to XR emission. This could be due to high energy photons interacting with ionospheric constituents, causing an enhancement of the ionization processes, and, consequently, electron density throughout the ionospheric layers. Nonetheless, high energy photons, such as HXR and GR emission, are expected to reach deeper into the ionosphere layers than lower energy photons, such as EUV and SXR emission (Mitra 1974; Tsurutani et al. 2009; Barta et al. 2019).

By examining the fmin daily profiles given in the Appendix, we notice that both of the GR and XR emissions of SFs can typically affect the ionosphere such that if the GR emission is delayed from the XR emission (delayed events), this leads to the appearance of two peaks in the fmin profile. However, if both emissions occur at almost the same time (simultaneous events), this leads to the appearance of only one peak.

To simplify the analysis and separate the response of the ionosphere to the GR flares from the XR flares, we divide the events into three categories: simultaneous (S-type), delayed (D-type) and not associated (N-type). The term "simultaneous event" refers to the GRF that was seen within ±20 minutes of the XRF start time, whereas "delayed event" refers to the GRF that began shortly before or within roughly two hours of the XRF end time. When a GRF event is not coupled with any XRF event within ±2 hr, it is termed a "not associated event".

Table 1
Some Characteristics of the GRFs and the Temporal Response of the Ionospheric Parameters

Flare's Date	Start Time (JST)	Exposure Time (min)	Flux (10^{-5} cm^{-2}s^{-1})	Fmin Peak (MHz)	Fmin Peak Time (JST)	Interval (hr)	Dfmin (MHz)
2011-03-08	11:33	43	3.23	6.92	13:00	1:27	3.96
2011-03-08	14:44	44	1.4	2.8	15:00	0:16	0.90
2011-08-04	13:55	42	2.3	4.96	15:00	1:05	2.73
2011-08-09	16:37	32	2.29	10.12	17:15	0:38	8.61
2011-09-07	7:11	36	22.8	4.16	7:30	0:19	1.15
2011-09-08	8:35	48	0.77	4.72	11:00	2:25	1.94
2012-01-23	13:06	40	1.12	4.4	14:00	0:54	2.49
2012-01-28	9:19	36	0.25	4	10:15	0:56	2.20
2012-03-05	13:07	42	0.58	6.36	14:30	1:23	2.63
2012-03-05	14:36	48	0.63	5.4	15:00	0:24	2.63
2012-03-07	11:26	18	75.1	10.12	12:15	0:49	2.44
2012-03-07	12:51	40	95.1	6.36	13:45	0:54	2.20
2012-03-09	14:12	43	0.27	4.64	15:00	0:48	2.11
2012-05-17	11:12	32	1.19	10.12	12:30	1:18	2.28
2012-05-17	12:49	30	0.44	5.4	14:00	1:11	2.24
2012-07-07	8:20	48	3.06	3.88	8:30	0:10	2.40
2012-10-23	13:13	30	0.73	5.52	13:30	0:17	2.58
2013-04-11	16:00	39	5.71	6.28	16:15	0:15	3.95
2013-05-13	13:31	43	0.96	4.04	13:45	0:14	1.42
2013-05-14	10:08	47	1.02	6.8	11:00	0:52	2.58
2013-05-14	11:43	47	3.3	5.28	12:00	0:17	3.16
2013-05-15	13:12	46	0.36	5.28	14:30	1:18	3.16
2013-10-11	15:56	42	12.5	2.92	16:45	0:49	1.39
2014-02-25	10:09	20	169.6	6.04	11:00	0:51	3.41
2014-02-25	13:20	20	28.3	5.32	14:30	1:10	2.35
2014-06-11	18:06	24	0.99	2.8	18:15	0:09	1.34
2015-06-21	11:09	33	0.25	9.12	11:45	0:36	1.53
2017-09-06	17:51	28	1.31	2.2	18:15	0:24	0.68
2017-09-07	8:05	26	0.96	2.8	8:45	0:40	1.15
2017-09-07	9:36	35	0.62	3.52	10:45	1:09	1.32

In Table 2, we list the classification of the 30 LAT-GRF events that have been discussed in this article.

3.1. The Impact of S-type GRFs on the Ionosphere

In the case of an S-type GRF, we observe a strong ionospheric disturbance. Figure 1 illustrates two examples of such type that occurred on 2011 August 9 (left panel) and 2013 April 11 (right panel). The GR emission starts at 16:37 JST and ends at 17:09 JST, while the XR emission starts at 16:48 JST and ends at 17:08 JST during the event on 2011 August 9. On 2013 April 11, the GR emission starts at 16:00 JST and ends at 16:39 JST, while the XR emission starts at 15:55 JST and ends at 16:29 JST. In both cases there is an obvious improvement in the fmin profiles above their associated background profiles at the times of both events. The fmin peak value is 10.12 MHz and detected at 17:15 JST for the first event day, while it is 6.28 MHz and recorded at 16:15 JST for the second event day. In fact, we cannot distinguish between the effect of GR and XR emissions in such events because their influence appears to blend and becomes a single peak in the fmin daily profile.

3.2. The Impact of D-type GRFs on the Ionosphere

Figure 2 shows two examples of D-type GRFs that occurred on 2011 September 8 (left panel) and 2013 May 15 (right panel), in which the GR emission from both flares begins after the XR emission from the same events has ended. The XR emission begins at 07:32 JST and finishes at 07:44 JST on 2011 September 8, whereas the GR emission begins at 08:35 JST and ends at 09:23 JST. On 2013 May 15 the XR emission begins at 10:25 JST and ends at 10:58 JST, while the GR emission begins at 13:12 JST and ends at 13:58 JST. This resulted in the appearance of two consecutive peaks in the fmin daily profiles, one associated with the XR emission and the other with the GR emission. For the event on 2011 September 8, the fmin peak values for XR and GR emissions occurred at 08:45 JST (5.8 MHz) and 11:00 JST (4.7MHz), respectively, whereas for the event on 2013 May 15, the induced fmin peak

Table 2
The Division of GRFs into Three Categories, According to their Association with the GOES XRFs

Flare's Date/Type	Simultaneous (S)			Delayed (D)			Not Associated (N)
	GRF start-end times (JST)	XRF start-end times (JST)	GOES class	GRF start-end times (JST)	XRF start-end times (JST)	GOES class	GRF start-end times (JST)
2011-03-08 N							11:33-12:16
2011-03-08 N							14:44-15-27
2011-08-04 D				13:55-14:37	12:41-13:04	M9.3	
2011-08-09 S	16:37-17:09	16:48-17:08	X6.9				
2011-09-07 S	07:11-7:47	07:12-07:24	X2.1				
2011-09-08 D				08:35-09:23	07:32-07:44	X1.8	
2012-01-23 D				13:06-13:46	12:38-13:34	M8.7	
2012-01-28 N							09:19-09:55
2012-03-05 D				13:07-13:49	11:30-13:43	X1.1	
2012-03-05 N							14:36-15:24
2012-03-07 D				11:26-11:45	09:02-09:40	X5.4	
2012-03-07 N							12:51-13:31
2012-03-09 D				14:12-14:55	12:22-13:18	M6.3	
2012-05-17 D				11:12-11:44	10:25-11:14	M5.1	
2012-05-17 N							12:49-13:18
2012-07-07 S	08:20-09:08	08:01-08:14	X1.1				
2012-10-23 D				13:13-13:43	12:13-12:21	X1.8	
2013-04-11 S	16:00-16:39	15:55-16:29	M6.5				
2013-05-13 D				13:31-14:14	10:53-11:32	X1.7	
2013-05-14 D				10:08-10:55	09:00-10:20	X3.2	
2013-05-14 N							11:43-12:31
2013-05-15 D				13:12-13:58	10:12-10:58	X1.2	
2013-10-11 S	15:56-16:39	16:01-16:45	M4.9				
2014-02-25 D				10:09-10:29	09:39-10:03	X4.9	
2014-02-25 N							13:20-13:40
2014-06-11 S	18:06-18:30	17:59-18:10	X1.0				
2015-06-21 S	11:09-11:42	11:04-12:15	M2.7				
2017-09-06 S	17:51-18:19	17:57-18:17	X2.2				
2017-09-07 N							08:05-08:31
2017-09-07 N							09:36-10:11

values due to XR and GR emissions occurred at 11:45 JST (8.1 MHz) and 14:30 JST (5.3 MHz), respectively.

3.3. The Impact of N-type GRFs on the Ionosphere

Figure 3 shows two examples of the effect of the N-type GRF on the lower ionosphere. Both events occurred on 2013 May 14 (left panel) and 2017 September 7 (right panel). In the left panel, the fmin daily profile indicates three successive emissions during this day. The first peak is attributed to GOES-XRF at 09:00-10:25 JST, while the second and third peaks are attributed to the LAT-GRFs at 10:08-10:55 JST and 11:43-12:31 JST, respectively. The GR emission attributed to the second peak is defined as D-type, while that related to the third peak is defined as N-type because it is not associated with XR emission. In the right panel, the first pair of peaks is attributed to the GR emissions, while the second and third pairs of peaks are attributed to the GBM and GOES XR emissions, respectively. The first LAT event starts at 8:05 JST, while the second at 09:36 JST. The corresponding fmin peak values for these LAT events are 2.8 MHz and 3.5 MHz, which occurred at around 08:45 JST and 10:45 JST, respectively.

3.4. Diurnal Variation Effect on the Fmin Daily Profiles

The diurnal variation in the fmin temporal profiles is clearly obvious, with a typical increase in their values approximately within two hours, from 11:00 to 13:00 JST, as shown in Figures 1, 2 and 3 for both the event and reference days. As a result, the diurnal variation gives a false indication of the ionospheric response to GRFs that occur during the noon times compared to those occurring away from the noon times, typically toward sunrise and sunset times. Figure 4 (left panel) features the case when the event occurs at noon (2011 March 8), while Figure 4 (right panel) shows the case when the event occurs near sunset (2014 June 11). In the first case, the fmin parameter peaks at around 7.0 MHz, but in the second case, it peaks at around 3.0 MHz.

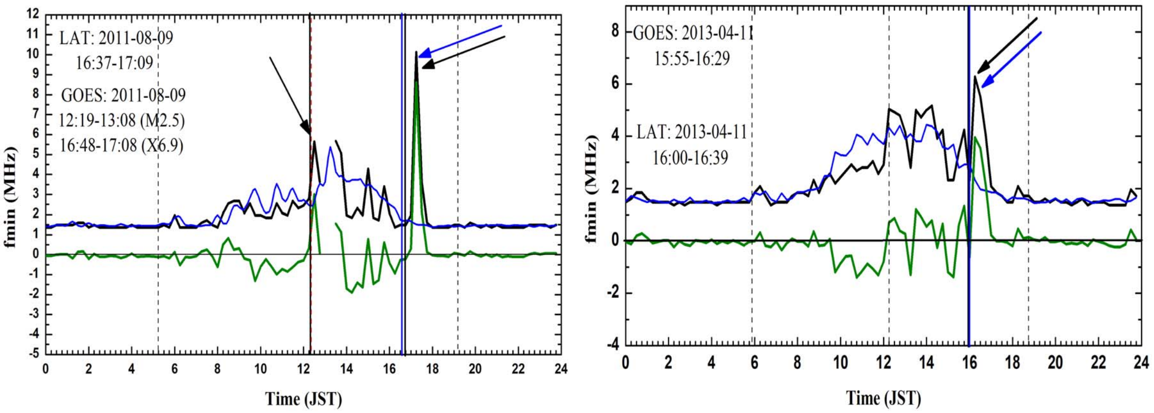

Figure 1. The response of the ionospheric parameter fmin to the S-type GRFs that occurred on 2011 August 9 (left) and 2013 April 11 (right). The dashed black vertical lines refer to the times of the sunrise, noon and sunset at the ionosonde station for the day of the event. The fmin daily variation profile, for the day of the event/events, and the reference background profiles are given in black and blue colors, respectively, while the residual profile is drawn in green. The blue and black arrows refer to the fmin peaks that are relevant to the effect of the LAT and GOES flares, respectively. The solid blue and black vertical lines indicate the start time of the LAT and GOES events, respectively.

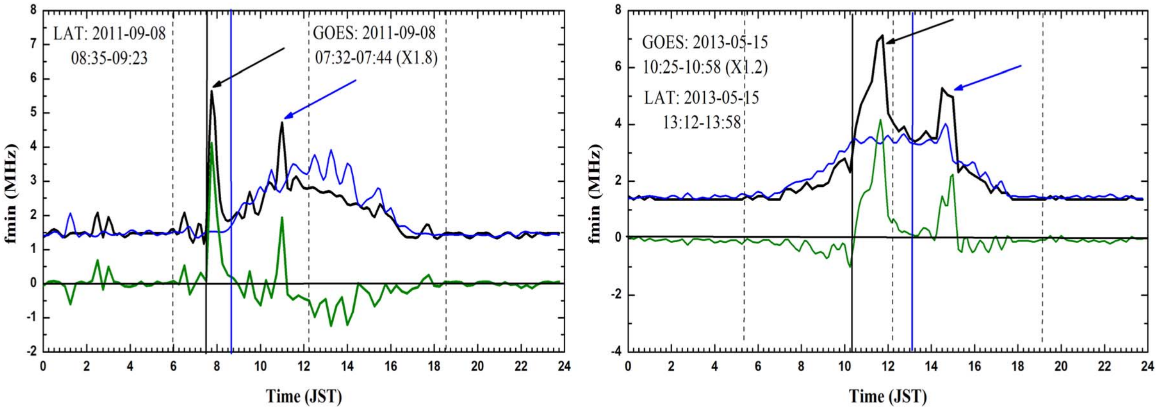

Figure 2. As Figure 1, but it shows the response of the ionospheric parameter fmin to the D-type GRFs that occurred on 2011 September 8 and 2013 May 15.

3.5. Global Effect of the GRFs and XRFs on the Fmin Values

To study the global effect of the GRFs and XRFs on the values of the fmin throughout the event days, we calculate the average fmin values during the daytime of each event day and those of the corresponding day of the previous year. The result is plotted in Figure 5, where the diagonal solid line indicates 1:1 matches. The results show that the average fmin values on all event days are higher than the corresponding day of the previous year (left panel). This result emphasizes the effect of GR emission, whether linked or not, with XR emission, on the ionization state of the D layer.

4. The Impact of Individual XRFs on the Ionosphere

For this study, we selected the GOES-XR events that were not associated with the LAT-GR emissions in the list of Ajello et al. (2021). All the graphs illustrated in Figure 6 affirm that XRFs have a significant impact on the fmin daily profiles and, in turn, the ionization processes in the D layer. Investigating the temporal profiles of fmin for the days of the flaring events reveals that there is a typical strong response for the fmin parameter to the individual XRFs, which is compatible with several studies such as Grubor et al. (2005) and Barta et al. (2019). Generally, a sudden increase in the values of fmin occurs just a few minutes after the start time of the XRF event. As an example, for the X3.3 event that happened on 2013 November 6 (upper left panel) at 07:07 JST, we found an enhancement in the fmin value of ∼3.0 MHz (07:15 JST) with respect to the reference profile, and for the X1.1 event that occurred on 2014 October 19 (lower left panel), there is an fmin enhancement of ∼10.0 MHz (13:45 JST) above the reference profile.

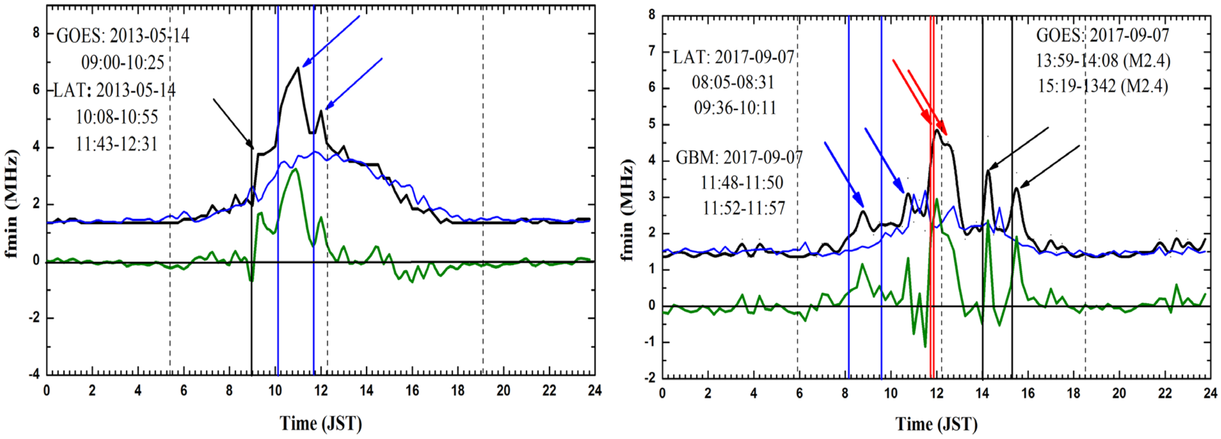

Figure 3. As Figure 1, but for the response of the ionospheric parameter fmin to the N-type GRFs that occurred on 2013 May 14 (left) and 2017 September 7 (right). The red arrows and vertical lines indicate the fmin peaks that are relevant to the effect of the GBM and the start time of the GBM events, respectively.

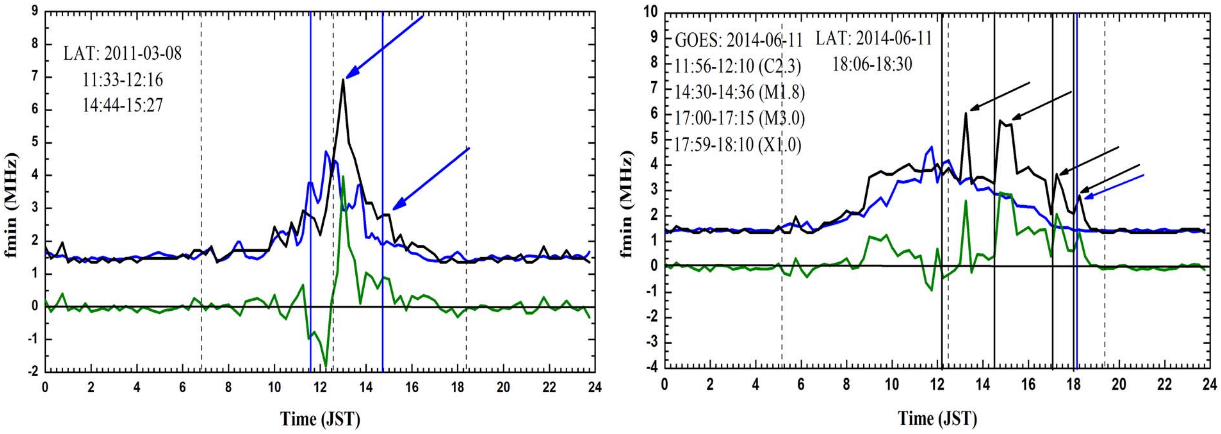

Figure 4. As in Figure 1, but for the impact of two GRF events on fmin peaks: one happens during noon time (left) and the other occurs near sunset (right).

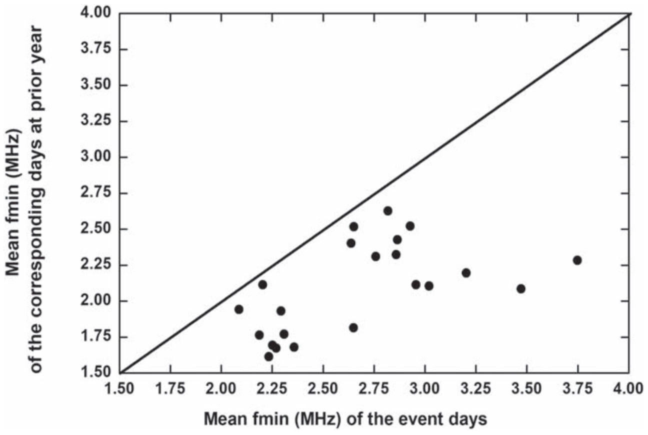

Figure 5. Comparison between the average fmin values, during the daytime, on the event days and the corresponding days of the preceding year. The diagonal solid line indicates 1:1 matches.

5. The Effect of GRF Characteristics on the Fmin Peak Value

We examine the influence of the GRF flux and photon index on the dfmin and fmin peak values. There is a moderate correlation between the GR emission flux and the dfmin and fmin peak values for the N-type. In addition, there is a good correlation between the dfmin and photon index values for the N-type. Table 3 lists the median values of the GRF flux, the average dfmin values and the average fmin time intervals of the three GRF classes. The results show that the S- and D-types have median GR fluxes of $\sim 2.7 \times 10^{-5}$ and $\sim 2.5 \times 10^{-5}$ $\mathrm{cm}^{-2}\mathrm{s}^{-1}$, respectively, which are higher than the N-type ($\sim 1.2 \times 10^{-5}$ cm^{-2} s^{-1}). Further, the average dfmin values of the S-type (∼2.6 MHz) and D-type (∼2.5 MHz) are larger than those of the N-type (∼2.2 MHz). Furthermore, there is a clear tendency for the average dfmin values to increase with the

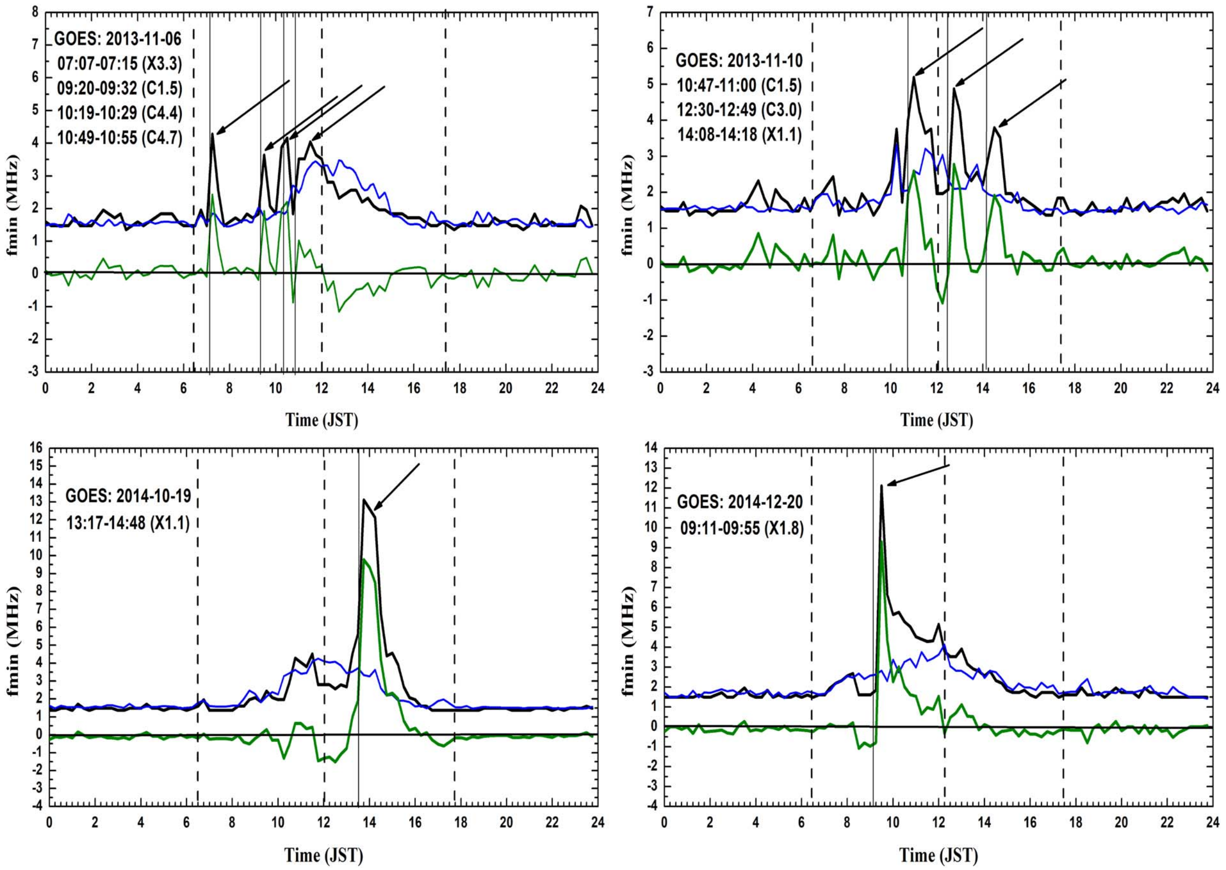

Figure 6. The temporal profiles of fmin for four XRF events that are not associated with any LAT detection of GR emissions. The description of the figure is the same as given in Figure 1.

median flux values from N-type to D-type to S-type, indicating that the XRF effect predominates in the case of association with GRFs. In other words, the flux of XRFs has a stronger influence on the electron density enhancement than that of GRFs.

6. Comparing the Impact of GR and XR Emission on the Ionosphere

6.1. Occurrence of GRFs and XRFs

The development of multi-wavelength band observations of SFs allows the detection of temporal emissions during the various SF stages. The XR and GR emissions represent the high energy part of the spectrum, and their emissions reflect specific mechanisms that occur during the SF stages. The XR flux measurements were taken a long time ago. Its first long-term observation was made in 1957 by the Sputnik 2 spacecraft. The first space telescope of the GOES series, designed to continuously monitor the SXR emission, was launched in 1975. The most important results about the flare's source geometry, however, came from detecting SXR and HXR emissions by the Yohkoh (1991–2001) and RHESSI (2002–2018) satellites (Lysenko et al. 2020). On the other hand, the first detection of GRs in the energy range of up to 5 GeV was made by the Gamma-1 experiment in 1990. Later, the Konus-Wind (Aptekar et al. 1995), Fermi-GBM (Meegan et al. 2009) and Fermi-LAT (Atwood et al. 2009) missions provided solar observation data in the HXR and GR ranges. By

Table 3
Average Values of the GRF and Ionospheric Parameters for the S-, D- and N-type GRFs

Type of GRF	Median Flux 10^{-5} cm^{-2} s^{-1}	Average dfmin Value (MHz)	Average Interval of fmin peak value (min)
N-type	1.2	2.2	50
D-type	2.5	2.5	64
S-type	2.7	2.6	25

Note. * We take the median GR flux, instead of the average, because there are many extreme values.

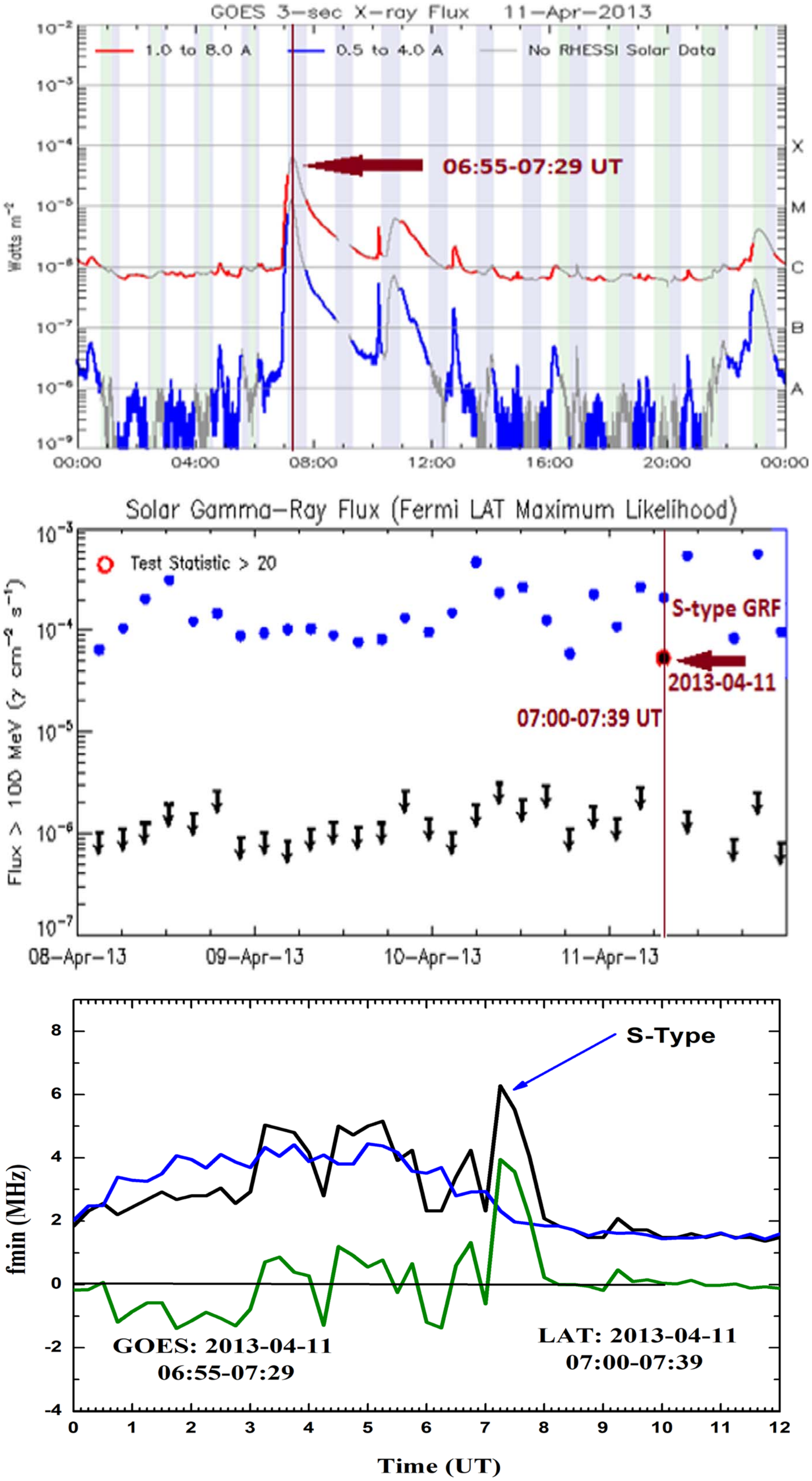

Figure 7. An example of the S-type GRF that occurred on 2013 April 11. The upper, middle and lower panels indicate, respectively, the GOES XR flux profile, the 4-day Fermi-LAT GR flux profile and the fmin daily profile. The times presented in the three panels are given in UT. The upper and middle graphs are subtracted from the Fermi SF XR and GR Observations website at https://hesperia.gsfc.nasa.gov/fermi_solar/.

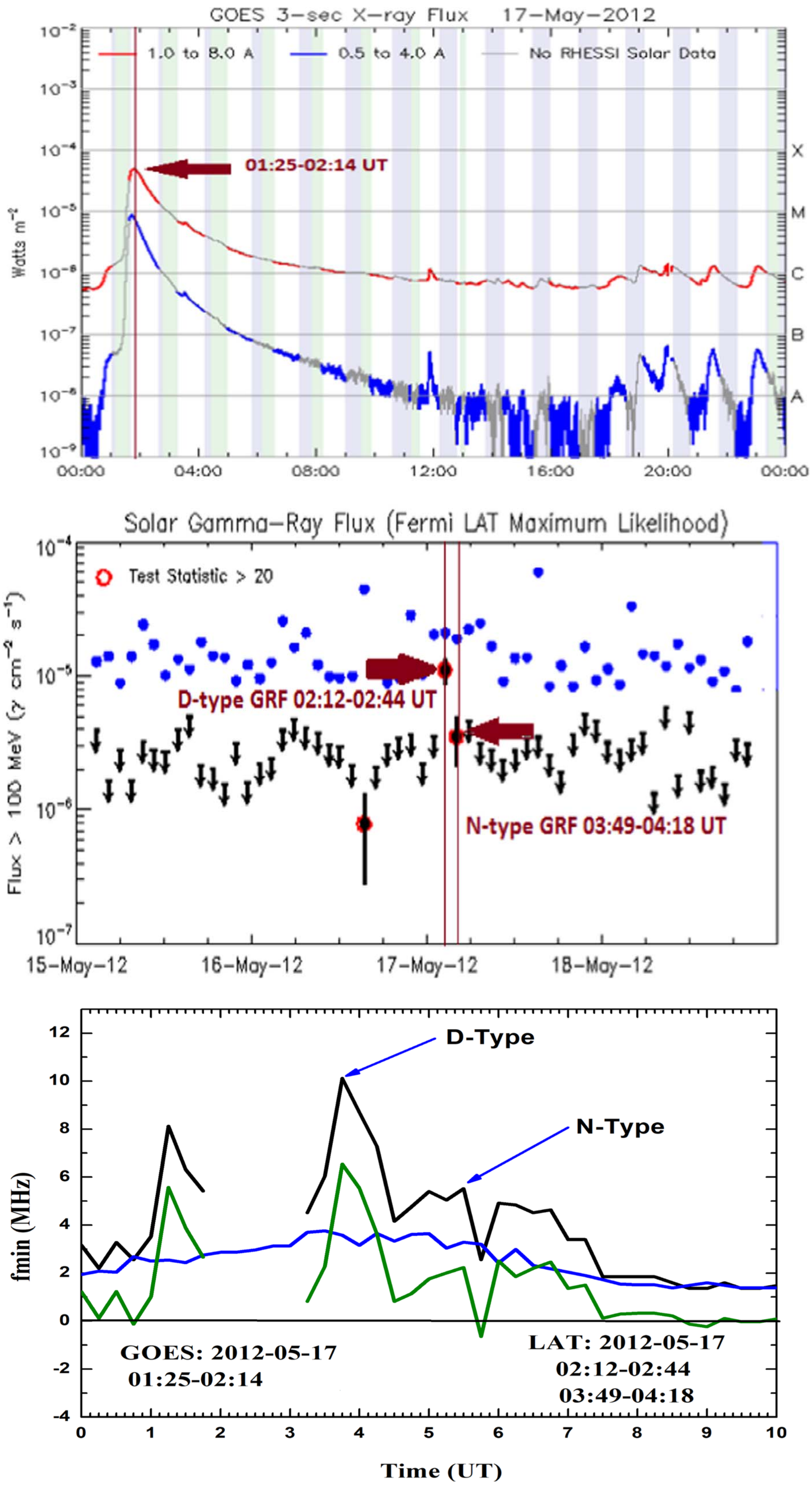

Figure 8. As Figure 7 but for the D- and N-type GRFs that occurred on 2012 May 17.

analyzing the SFs and their various emissions over the last few solar cycles, a few researchers found that the fluxes of the GRFs and XRFs are not well correlated. According to Ajello et al. (2021), based on Fermi-LAT data, high energy GR emission (100 MeV) is not correlated with the intensity of XRFs. Vestrand et al. (1999) discovered GR emission lines in the spectra of only 67 of the 258 flares of class C1.0 and higher, whereas Ackermann et al. (2014) discovered GR emissions only in M- and X-class flares.

Our classification of the impacting GRFs on the lower ionosphere conveniently corresponds to the actual SF phases. The S-type GRFs are flares that occur during the impulsive phase of XRFs, and are referred to by Ajello et al. (2021) and Lysenko et al. (2020) as prompt flares and impulsive phase flares, respectively. There are also D-type GR flares, which are extended late-phase flares (Lysenko et al. 2020) or delayed flares (Ajello et al. 2021), in which the GR emission follows the impulsive phase and can persist for a few minutes to several hours. The N-type GRFs are either events with no GOES-XR emission detection or events with a much extended late phase.

Figure 7 displays an example of an S-type GRF expressing impulsive phase (prompt) flares. This event occurred on 2013 April 11, with the start and end times of the GOES detection being 06:55 UT and 07:29 UT (upper panel) and the Fermi-LAT detection being 07:00 UT and 07:39 UT (middle panel) respectively. Figure 7 (lower panel) shows the daily fmin profile for the same day, indicating a strong impact as a single peak in the fmin profile.

Figure 8 shows an example of the D-type GRF and another for the N-type GRF. Both events took place on the same day, 2012 May 17. According to our classification, the first event is defined as a D-type GRF, also known as an extended late-phase flare or delayed phase flare in the literature. Figure 8 illustrates the GOES-XR emission at start/end periods of 01:25-2:02:14 UT, which include the impulsive phase. The LAT-GR emission has a 2:12-2:44 UT start/end time (middle panel). Another GR emission, which reflects the N-type GRF, has start/end times of 03:49-04:18 UT (middle panel), which is more than two hours after the GOES-XR emission. The fmin profile that is drawn in Figure 8 (lower panel) refers to two induced peaks that represent two independent effects on the D-layer ionization levels.

6.2. Similarities and Discrepancies of the Ionospheric Responses to the GRFs and XRFs

We found that both GRFs and XRFs have an impact on the lower ionosphere, or D-region. The GR emission is found to be most likely shifted or delayed from the XR impulsive peak (Ajello et al. 2021). This has an effect on the ionospheric response, which has a significant temporal enhancement in the fmin values due to XR emission, as well as an additional enhancement due to GR emission. When GR emission occurs during the impulsive phase of XR emission, it typically manifests as a single strong peak in the fmin values, whereas when GR emission occurs after the impulsive phase, there will be a distinct peak due to this emission rather than that of the XR emission.

In fact, unlike their HXR emission, the GR emission of SFs is a superposition of several components, including contributions from both ultra-relativistic electrons, which generate the bremsstrahlung continuum, and accelerated ions, which are observed via the emission from nuclear reactions in the solar atmosphere. However, GR emission from flaring regions is weak in comparison to XR emission (Lysenko et al. 2020). As a result, the consequent ionospheric response to XRFs is expected to be stronger than that to GRFs. This is consistent with our findings, which show that the impacting XRFs cause spikes or strong peaks in fmin values within a short time interval, whereas the GRF induced peaks are typically weak and take a longer time interval to appear. Furthermore, we found that the ionospheric reaction to GR emission varies in duration, with some taking longer intervals of time than others. We noticed a delay of more than one hour in the fmin parameter's response to nine of the 30 GR events listed in Table 1. Moreover, one of them takes longer than two hours (2011-09-08, Figure 2). All of these events are classified as D- and N- GRF types. This time delay in the ionospheric response to GRFs is most likely attributed to the weak flux of GR emissions and their timescale which tends to mirror the position of the flare itself on the Sun, whether it is a limb or disk flare. Matsumoto et al. (2005) reported that the limb flares have stronger GR emission than disk ones due to the energy-dependent anisotropy. Because the electron bremsstrahlung emissivity is relativistically forward-peaked, GR photons from a disk flare would have to be Compton back-scattered to reach us, and therefore lose a larger fraction of their energy than those from limb flares.

We also noticed that if the GRF occurs close to sunrise or sunset, the induced fmin peak is most likely to be weak. The induced fmin peaks, on the other hand, are most likely to be strong when the impacting GRF occurs near noon. This is because the solar zenith angle of the ionosonde station is at its greatest during the noon hour. The situation is similar for the influencing XRFs.

7. Conclusions

SFs release high-energy particles and electromagnetic radiation across a broad spectrum, from low-energy radio waves to high-energy XRs and GRs, which disrupt our planet's ionospheric layer and, as a result, the Earth's space environment-based technologies. The radio signal attenuation and loss in the space environment are more likely related to the enhancement of electron concentration in the Earth's ionosphere. In this article, we studied the influence of the solar

GRFs and XRFs on the Earth's lower ionosphere by displaying the possible variation of the daily profile of lower ionospheric parameter fmin.

To clarify the effect of the Fermi-LAT GRFs on Earth's ionosphere, which is considered to be the first ever study, we used a sample of 30 GRFs that occurred over the course of 23 days, spanning between 2011 and 2017. According to their association with the GOES XRFs throughout the event days, we classified the GRF sample into three types: not associated (10 events); simultaneous (8 events); and delayed (12 events). These GRF types reflect their actual timing evolution with respect to their associated XRFs.

In general, we found that the response of the ionospheric parameter fmin, which expresses the electron concentration in the lower ionosphere, is stronger for the impacting XRFs than that for the impacting GRFs. Moreover, dfmin responses are so different according to the type of GRF, where the S-type events cause just a single spike in the fmin daily profile and two peaks in the case of the D-type. Moreover, we noticed that dfmin values are more significant than fmin peak values, particularly when comparing the influence of different LAT-GRF types on fmin daily profiles. The average dfmin value for the S-type (2.6 MHz) is slightly higher than that for the D-type (2.5 MHz), and both are significantly higher than the N-type (1.2 MHz). This shows that the influence of XRFs on the fmin daily profile is stronger than the GRFs in the case of association with GRFs (S- and D-types).

Further regarding the impact of the LAT-GR and GOES-XR emissions on the ionosphere, we found the diurnal variation affects the temporal profiles of the ionospheric parameters so clearly that during the day the values of fmin have low values near sunrise and sunset times and maximize around noon time.

Acknowledgments

The authors extend their appreciation to the Deputyship for Research & Innovation, Ministry of Education in Saudi Arabia for funding this research work through the project number (MoE-IF-20-02/05). This research draws upon data provided by WDC for Ionosphere and Space Weather, Tokyo, National Institute of Information and Communications Technology. We acknowledge the use of the Fermi Solar Flare Observations facility funded by the Fermi GI program ("https://hesperia.gsfc.nasa.gov/fermi_solar/").

Appendix

In the present section, we exhibit the full fmin profiles of the entire events discussed in this article (Figure A1). As illustrated in Figure 1, the fmin daily variation profile for the event/events day, as well as the reference background profiles, is shown in black and blue, respectively, while the difference between both profiles is depicted in green. The blue, red and black arrows represent the fmin peaks related to the effect of the LAT, GBM and GOES flares, respectively. The start times of the LAT, GBM and GOES events are indicated by solid blue, red and black vertical lines, respectively. We present here the response of the fmin profiles for the 30 GRFs that occurred on 23 event days spanning from 2011 to 2017.

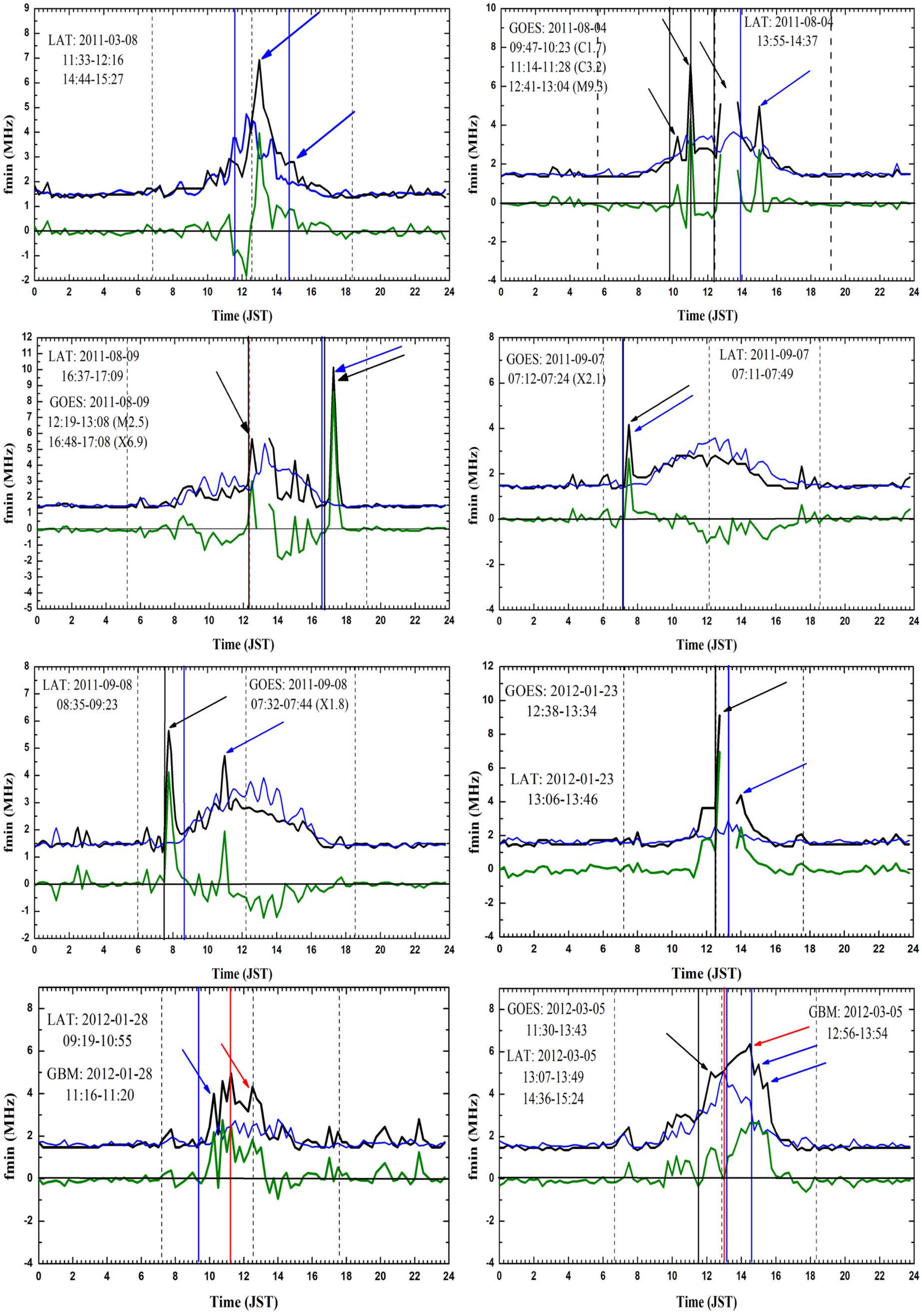

Figure A1. The daily profiles of the fmin ionospheric parameters during the 23 event days. The description of the figure is the same as given in Figure 1.

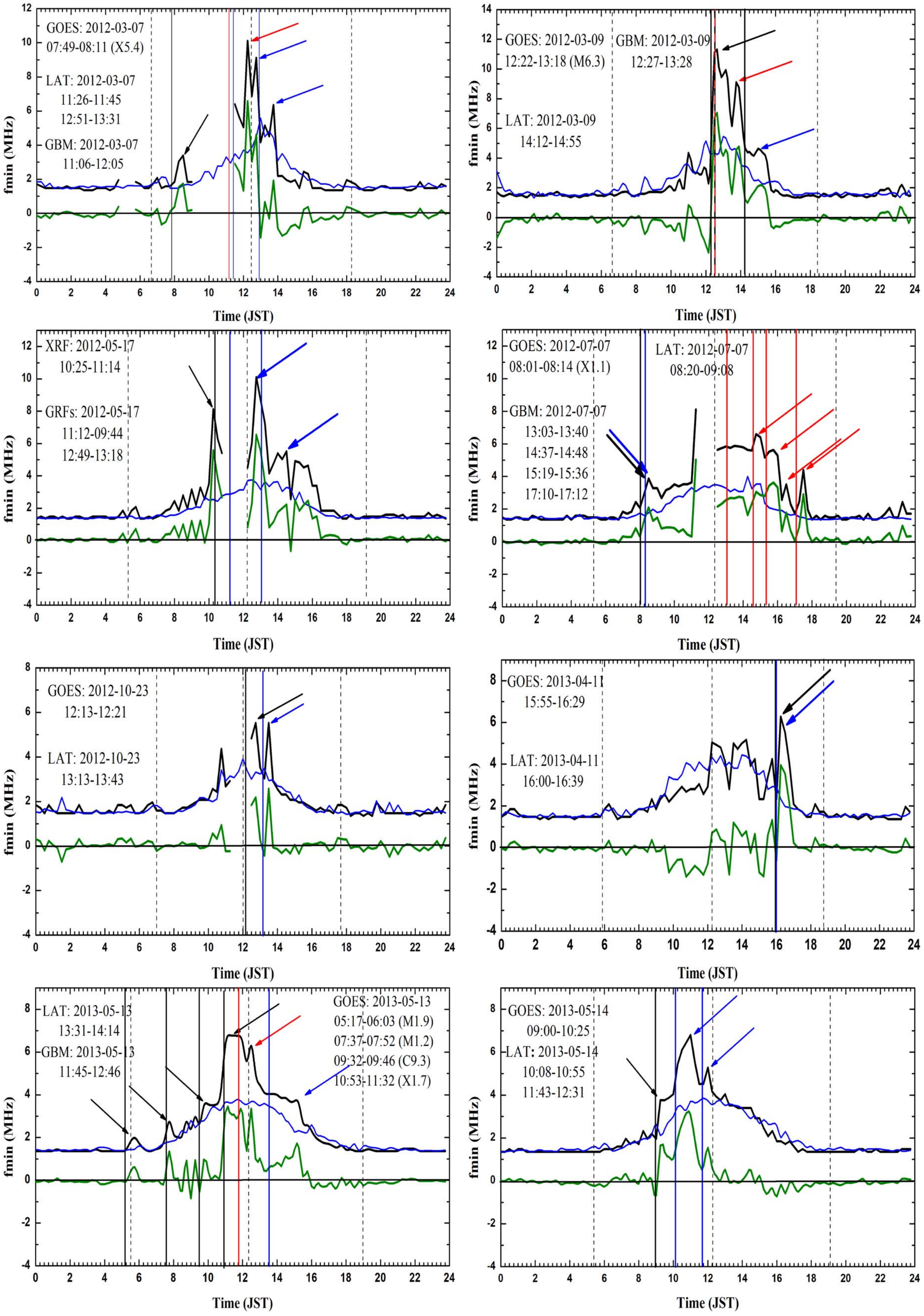

Figure A1. (Continued.)

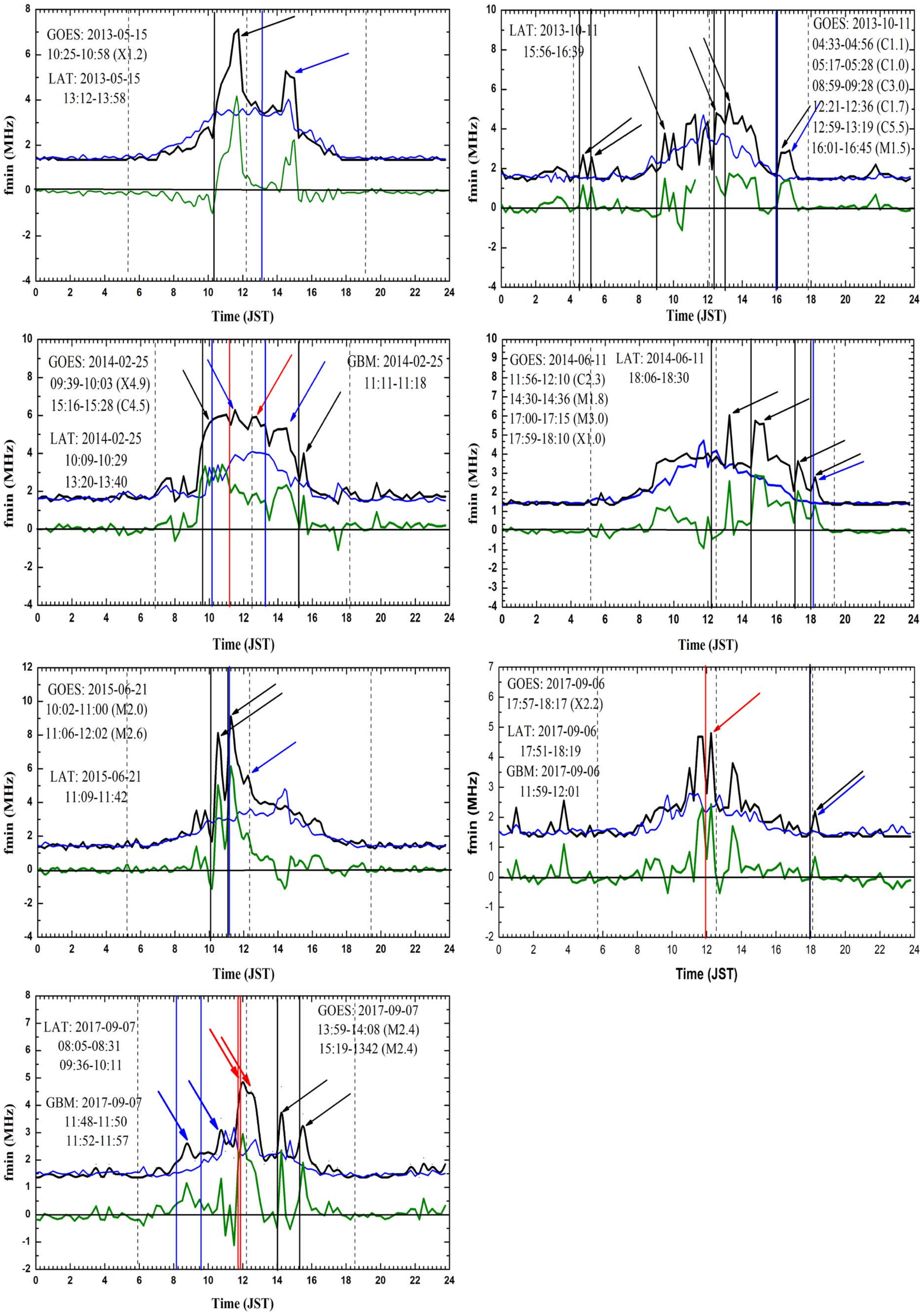

Figure A1. (Continued.)

ORCID iDs

Hussein M. Farid https://orcid.org/0000-0001-5320-1525
Alaa Ali https://orcid.org/0000-0003-4180-8420

References

Ackermann, M., Ajello, M., Albert, A., & Allafort, A. 2014, ApJ, 787, 15
Ackermann, M., Ajello, M., Allafort, A., & Atwood, W. B. 2012, ApJ, 745, 144
Ajello, M., Albert, A., Allafort, A., & Baldini, L. 2014, ApJ, 789, 20
Ajello, M., Baldini, L., Bastieri, D., & Bellazzini, R. 2021, ApJS, 252, 13
Aptekar, R. L., Frederiks, D. D., Golenetskii, S. V., et al. 1995, SSRv, 71, 265
Atwood, W. B., Abdo, A. A., Ackermann, M., et al. 2009, ApJ, 697, 1071
Barta, V., Sátori, G., Berényi, K. A., Kis, Á., & Williams, E. 2019, AnGp, 37, 747
Bello, V., Sátori, G., Berényi, K. A., Kis, Á., & Williams, E. 2017, Ilorin Journal of Science, 4, 139
Chupp, E. L., Forrest, D. J., Ryan, J. M., et al. 1982, ApJL, 263, L95
Chupp, E. L., & Ryan, J. M. 2009, RAA, 9, 11
Farid, H. M., Mawad, R., Ghamry, E., & Yoshikawa, A. 2020, Univ, 6, 200
Farid, H. M., Mawad, R., Yousef, M., & Yousef, S. 2015, Elixir Space Sci, 80, 31067
Forrest, D. J., Vestrand, W. T., Chupp, E. L., et al. 1985, in Int. Cosmic Ray Conf., 4, 19th Int. Cosmic Ray Conf. (ICRC19), 146
Forrest, D. J., Vestrand, W. T., Chupp, E. L., et al. 1986, AdSpR, 6, 115
Grubor, D., Sulic, D., & Zigman, V. 2005, SerAJ, 171, 29
Guyer, S., & Can, Z. 2013, in 2013 6th Int. Conf. on Recent Advances in Space Technologies (RAST), 729
Hargreaves, J. K. 1992, The Solar-terrestrial Environment. An Introduction to Geospace—the Science of the Terrestrial Upper Atmosphere, Ionosphere and Magnetosphere (Cambridge: Cambridge Univ. Press)
Inan, U. S., Lehtinen, N. G., Moore, R. C., et al. 2007, GeoRL, 34, L08103
Kafexhiu, E., Romoli, C., Taylor, A. M., & Aharonian, F. 2018, ApJ, 864, 148
Kouloumvakos, A., Rouillard, A. P., Share, G. H., et al. 2020, ApJ, 893, 76
Lysenko, A. L., Frederiks, D. D., Fleishman, G. D., et al. 2020, PhyU, 63, 818
Matsumoto, Y., Makishima, K., Kotoku, J., et al. 2005, PASJ, 57, 211
Meegan, C., Lichti, G., Bhat, P. N., et al. 2009, ApJ, 702, 791
Meeus, J. 1998, Astronomical Algorithms (Richmond, VA: Willmann-Bell, Inc.)
Mitra, A. P. 1974, Ionospheric Effects of Solar Flares, Vol. 46
Moldwin, M. 2008, An Introduction to Space Weather (Cambridge: Cambridge Univ. Press)
Qian, L., Wang, W., Burns, A. G., et al. 2019, JGRA, 124, 2298
Ryan, J. M. 2000, SSRv, 93, 581
Tanaka, Y. T., Terasawa, T., Yoshida, M., Horie, T., & Hayakawa, M. 2008, JGRA, 113, A07307
Tripathi, S. C., Khan, P. A., Ahmad, A., et al. 2011, in Proc. IEEE Int. Conf. on Space Science and Communication (IconSpace), 134
Tsurutani, B. T., Verkhoglyadova, O. P., Mannucci, A. J., et al. 2009, RaSc, 44, RS0A17
Vestrand, W. T., Forrest, D. J., Levenson, K. A., et al. 1999, in AIP Conf. Ser., 499, Small Missions for Energetic Astrophysics, ed. S. P. Brumby (Melville, NY: AIP), 156
Vilmer, N., MacKinnon, A. L., Trottet, G., & Barat, C. 2003, A&A, 412, 865
Yamauchi, M., Sergienko, T., Enell, C. F., et al. 2018, SpWea, 16, 1437